

# Infrared background signatures of the first black holes

Bin Yue<sup>1</sup>, Andrea Ferrara<sup>2</sup>, Ruben Salvaterra<sup>3</sup>, Yidong Xu<sup>1</sup>, Xuelei Chen<sup>1,4</sup>

## ABSTRACT

Angular fluctuations of the Near InfraRed Background (NIRB) intensity are observed up to scales  $\lesssim 1^\circ$ . Their interpretation is challenging as even after removing the contribution from detected sources, the residual signal is  $> 10$  times higher than expected from distant galaxies below the detection limit and first stars. We propose here a novel interpretation in which early, intermediate mass, accreting direct collapse black holes (DCBH), which are too faint to be detected individually in current surveys, could explain the observed fluctuations. We find that a population of highly obscured ( $N_{\text{H}} \gtrsim 10^{25} \text{ cm}^{-2}$ ) DCBHs formed in metal-free halos with virial temperature  $10^4 \text{ K}$  at  $z \gtrsim 12$ , can explain the observed level  $\approx 10^{-3} (\text{nW m}^{-2} \text{ sr}^{-1})^2$  of the  $3.6$  and  $4.5 \mu\text{m}$  fluctuations on scales  $> 100''$ . The signal on smaller scales is instead produced by undetected galaxies at low and intermediate redshifts. Albeit Compton-thick, at scales  $\theta > 100''$  DCBHs produce a CXB (0.5-2 keV)-NIRB ( $4.5 \mu\text{m}$ ) cross-correlation signal of  $\approx 10^{-11} \text{ erg s}^{-1} \text{ cm}^{-2} \text{ nW m}^{-2} \text{ sr}^{-1}$  slightly dependent on the specific value of the absorbing gas column ( $N_{\text{H}} \approx 10^{25} \text{ cm}^{-2}$ ) adopted and in agreement with the recent measurements by Cappelluti et al. (2012a). At smaller scales the cross-correlation is dominated by the emission of high-mass X-ray binaries (HMXB) hosted by the same low- $z$ , undetected galaxies accounting for small scale NIRB fluctuations. These results outline the great potential of the NIRB as a tool to investigate the nature of the first galaxies and black holes.

*Subject headings:* cosmology: diffuse radiation - early Universe - X-rays: diffuse background - galaxies

## 1. INTRODUCTION

Measurements of the Near InfraRed Background (NIRB) have raised the hope to open a new window on high redshift galaxies or even the first stars (Kashlinsky et al. 2002; Santos et al. 2002;

---

<sup>1</sup>National Astronomical Observatories, Chinese Academy of Sciences, 20A Datun Road, Chaoyang, Beijing 100012, China

<sup>2</sup>Scuola Normale Superiore, Piazza dei Cavalieri 7, I-56126 Pisa, Italy

<sup>3</sup>INAF, IASF Milano, via E. Bassini 15, I-20133 Milano, Italy

<sup>4</sup>Center of High Energy Physics, Peking University, Beijing 100871, China

Salvaterra & Ferrara 2003; Cooray et al. 2004; Kashlinsky et al. 2004). The observed NIRB fluctuations are largely dominated by low redshift galaxies which are either resolved individually or have their signal constrained by the luminosity functions obtained from deep multiband surveys (Helgason et al. 2012). However, even after subtraction of these contributions from the images, the majority of the residual signal is still unlikely to come from high redshift galaxies or first stars (Salvaterra & Ferrara 2006; Cooray et al. 2012a; Yue et al. 2013). As the fluctuation measurements have been confirmed by different experiments (Kashlinsky et al. 2005, 2007; Thompson et al. 2007; Matsumoto et al. 2011; Kashlinsky et al. 2012; Cooray et al. 2012b), the problem remains of what sources produce the measured signal (see Cooray et al. 2012b for an alternative explanation).

According to the most popular cosmological theory, the first stars formed at  $z = 20 - 30$  (Miralda-Escudé 2003) in mini-halos (dark matter structures with virial temperatures  $T_{\text{vir}} = 10^{3-4}$  K) cooling their primordial (metal-free) gas via  $\text{H}_2$  line emission. For a sufficiently intense Lyman-Werner band (LW  $\equiv 11.2 - 13.6$  eV) UV radiation field,  $\text{H}_2$  can be photo-dissociated (see e.g., Shang et al. 2010) and cooling and star formation are quenched. Larger halos ( $T_{\text{vir}} \gtrsim 10^4$  K) do not rely on  $\text{H}_2$ , as hydrogen  $\text{Ly}\alpha$  line emission and other processes sustain an almost isothermal collapse preventing gas fragmentation into smaller sub-units. Under these conditions, theoretical works (Shibata & Shapiro 2002; Bromm & Loeb 2003; Koushiappas et al. 2004; Begelman et al. 2006; Volonteri et al. 2008; Regan & Haehnelt 2009; Shang et al. 2010) show that the most likely outcome is a rapid ( $\approx 1$  Myr) formation of a direct collapse black hole (DCBH) of mass  $10^{4-6} M_{\odot}$  (Bromm & Loeb 2003; Lodato & Natarajan 2006; Begelman et al. 2006; Regan & Haehnelt 2009; Johnson et al. 2012a,b). The halo gas presumably continues to fall onto the BH thus powering its luminosity at the Eddington rate for 10-100 Myr. These DCBHs are very likely Compton-thick (implying H column densities  $N_{\text{H}} \gtrsim 10^{25} \text{ cm}^{-2}$ ), as the gas infall rate is very high and the stacked gas very compact. Compton-thick quasars are heavily absorbed from UV (above 13.6 eV) to X-ray energies, as ionizing photons are absorbed by neutral gas surrounding the BH (Gilli et al. 2007; Murphy & Yaqoob 2009) and reprocessed into optical-UV “nebular” emission (Fernandez & Komatsu 2006). Therefore, they do not contribute significantly to the reionization of the intergalactic medium. This rises the hope to explain the observed amplitude of the source-subtracted NIRB fluctuations by DCBHs, without overshooting the experimental constraints on the unresolved fraction of the Cosmic X-ray Background (CXB) (Salvaterra et al. 2012) and reionization.

Intermediate mass BH seeds such as those formed via the above mechanism, ease the problem of explaining the inferred masses,  $\sim 10^9 M_{\odot}$ , of supermassive BHs (SMBH; Petri et al. 2012) already in place at  $z = 6 - 7$  (Fan et al. 2001). In fact, starting from a smaller, stellar-size mass BH, accretion should proceed at the Eddington limit throughout the entire Hubble time to build up such a large mass. This seems unlikely.

The layout of the paper is as follows. In Section 2 we present the spectrum of a Compton-thick BH, and introduce the calculation of their contribution to the NIRB and the CXB. In Section 3 we present our results: the DCBH parameters that fit the measured NIRB fluctuations; the predictions

of CXB angular power spectrum and the CXB-NIRB cross-correlation. Conclusions are presented in Section 4. We discuss the possibility of the formation of a large number of DCBHs in Appendix A.

Throughout this paper, we use the same cosmological parameters as in Salvaterra et al. (2011):  $\Omega_m=0.26$ ,  $\Omega_\Lambda=0.74$ ,  $h=0.73$ ,  $\Omega_b=0.041$ ,  $n = 1$  and  $\sigma_8=0.8$ . The transfer function is from Eisenstein & Hu (1998). Magnitudes are given in the AB system.

## 2. Model description

### 2.1. Spectrum of a Compton-thick accreting BH

The primary emission spectrum of an accreting BH can be described as the sum of three components:

$$L_\nu = L_\nu^{\text{MBB}} + L_\nu^{\text{PL}} + L_\nu^{\text{refl}}, \quad (1)$$

namely a multicolor black body spectrum, i.e., a combination of black body spectra with different temperatures coming from different parts of the accretion disc; a power law spectrum from a surrounding hot corona; and a reflection component respectively. The first two components have comparable luminosity (Miller & Colbert 2004; Kuhlen & Madau 2005). The temperature of the disc decreases from inside out and is maximum in the innermost regions with (Makishima et al. 2000; Salvaterra et al. 2005)

$$T_{\text{max}} = \left( \frac{M_{\text{BH}}}{M_\odot} \right)^{-0.25} \text{ keV}, \quad (2)$$

where  $M_{\text{BH}}$  is the BH mass. This approximation is valid in the case the central object is a Schwarzschild BH, the innermost radius is  $\approx 5$  times the Schwarzschild radius, and the accretion reaches the Eddington limit. The spectral energy distribution is then (Mitsuda et al. 1984)

$$L_\nu^{\text{MBB}} = L_{\text{MBB}} \int_0^{T_{\text{max}}} B_\nu(T) \left( \frac{T}{T_{\text{max}}} \right)^{-11/3} \frac{dT}{T_{\text{max}}}, \quad (3)$$

where  $B_\nu(T)$  is the emission spectrum of a black body with temperature  $T$ ,  $L_{\text{MBB}}$  is a factor used for normalization.

The hot corona emission spectrum is usually parametrized as a power law with an exponential cut-off, i.e.

$$L_\nu^{\text{PL}} = L_{\text{PL}} \nu^{-\alpha_s} \exp(-h_p \nu / E_{\text{cut}}), \quad (4)$$

where  $h_p$  is the Planck constant. We adopt  $\alpha_s = 1$  and  $E_{\text{cut}} = 300$  keV (Sazonov et al. 2004). Again  $L_{\text{PL}}$  is the normalization factor. As in Salvaterra et al. (2005), the power-law is truncated below the peak of the disc component, i.e.  $\sim 3T_{\text{max}}$ .

A fraction of the radiation emitted by the hot corona is reflected by the disc, and must be added to the original spectrum. During this process, high energy photons would be Compton

scattered to lower energies, producing a “Compton hump” at energy around 30 keV (Fiocchi et al. 2007). We use the `pexrav` (Magdziarz & Zdziarski 1995) package included in `xspec`<sup>1</sup> to calculate this reflection component,  $L_\nu^{\text{refl}}$ , adopting an angle between the normal to the disc and the line-of-sight of  $60^\circ$ . The reflection scaling factor, i.e. the solid angle (in units of  $2\pi$ ) subtended by the disc as viewed from the X-ray source, is set equal to 1, which corresponds to the case of an isotropic source located above the disk (see `xspec` manual for more details). As DCBHs form in pristine gas, we adopt a zero gas metallicity.

Throughout this paper we assume that the BH radiates at the Eddington limit when accreting, so that its bolometric luminosity is  $L_{\text{Edd}} = 1.3 \times 10^{38} M_{\text{BH}} \text{ erg s}^{-1}$ , as done in many previous works (e.g., Madau et al. 2004; Cooray & Yoshida 2004; Alvarez et al. 2009; McQuinn et al. 2009; Park & Ricotti 2011). However, our results do not depend critically on this assumption as a smaller Eddington ratio can be compensated (up to a certain point) by longer accretion times.  $L_{\text{MBB}}$  and  $L_{\text{PL}}$  are then determined by  $\int L_\nu^{\text{MBB}} d\nu = \int L_\nu^{\text{PL}} d\nu$  and  $\int (L_\nu^{\text{MBB}} + L_\nu^{\text{PL}} + L_\nu^{\text{refl}}) d\nu = L_{\text{Edd}}$ . As an example, we plot the final primary spectrum of a BH with mass  $10^6 M_\odot$  and its three components in the upper panel of Fig. 1. The reflection spectrum only contributes  $\approx 10\%$  of the total energy.

As DCBHs are enshrouded by a massive accreting envelope, it is very likely that they are Compton-thick. In this case, the emerging spectrum, filtered by such medium, will be quite different from the primary one. In fact, most of the photons above 13.6 eV are either absorbed or scattered. We assume that the absorbing gas distribution is spherically symmetric, so that also the reflection component is absorbed. This is motivated by the fact metal-free gas disks are relatively hot and in  $T_{\text{vir}} > 10^4$  K halos are likely to be fat (Volonteri & Rees 2005). With the primary spectrum expressed by Eq. (1), we follow the Yaqoob (1997) (Y97) to calculate the absorbed and scattered spectrum,  $L_\nu^{\text{abs}}$ , despite of possible uncertainties arising when  $N_{\text{H}} > 5 \times 10^{24} \text{ cm}^{-2}$ . A brief introduction of the method and formulae is given in Appendix B, we refer interested readers to the original paper for more details. The  $L_\nu^{\text{abs}}$  of a  $10^6 M_\odot$  BH with  $N_{\text{H}} = 1.5 \times 10^{25} \text{ cm}^{-2}$  is shown in the bottom panel of Fig. 1.

The energy of photons is transferred to electrons by both photoelectric absorption and Compton scattering. While each UV photon typically ionizes only one neutral atom, we have to take into account that each X-ray photon generates a high energy electron directly, which in turn initiates a collisional ionization cascade. The total number of ionizations per unit time is

$$Q_{\text{H}} = Q_{\text{H,UV}} + Q_{\text{H,X}}, \quad (5)$$

where the contribution of UV ionization is

$$Q_{\text{H,UV}} = \int_{\nu_{\text{H}}}^{\nu_{\text{X}}} \frac{L_\nu - L_\nu^{\text{abs}}}{h_p \nu} d\nu, \quad (6)$$

---

<sup>1</sup><http://heasarc.nasa.gov/xanadu/xspec/>

while the contribution of X-ray ionization is

$$Q_{\text{H,X}} \approx \int_{\nu_{\text{X}}}^{\infty} \frac{L_{\nu} - L_{\nu}^{\text{abs}}}{h_{\text{p}}\nu} d\nu + \frac{1}{3} \int_{\nu_{\text{X}}}^{\infty} \frac{L_{\nu} - L_{\nu}^{\text{abs}}}{h_{\text{p}}\nu} \left( \frac{\nu}{\nu_{\text{H}}} - 1 \right) d\nu, \quad (7)$$

where  $\nu_{\text{H}}$  is the frequency of photons with energy 13.6 eV;  $\nu_{\text{X}}$  is the frequency of the lowest energy X-ray photons (equal to 200 eV in this work); The 1/3 factor in the second term of the right hand side takes into account the fact that, for a neutral gas, about one third of the energy of the high energy electrons goes into the collisional ionization (Chen & Kamionkowski 2004; Valdés & Ferrara 2008). Eq. (7) implicitly assumes that the collisional ionization is faster than the production rate of free electrons by photons. This is always true if the density of the neutral material is sufficiently large, as in the case considered here. If  $N_{\text{H}} = 1.5 \times 10^{25} \text{ cm}^{-2}$ , for BHs with mass  $10^5$  ( $10^6$ )  $M_{\odot}$ ,  $Q_{\text{H}} \approx 1.7 \times 10^{53} \text{ s}^{-1}$  ( $1.8 \times 10^{54} \text{ s}^{-1}$ ).

Under these conditions, the absorbed part of the spectrum,  $(L_{\nu} - L_{\nu}^{\text{abs}})$ , will finally escape from the Compton-thick material as the form of “nebular emission”, including the free-free, free-bound emission, and the two-photon emission. The Ly $\alpha$  emission is not included here, as the hydrogen density is large enough that the Ly $\alpha$  photons are resonantly trapped in the surrounding gas (Xu et al. 2011; Spaans & Silk 2006; Schleicher et al. 2010; Latif et al. 2011); in this case the system is not able to lose energy through Ly $\alpha$  emission, instead, essentially all the  $n = 2$  to  $n = 1$  transitions will eventually produce two-photon emission (Brown & Mathews 1970; Schleicher et al. 2010).

The luminosity of free-free and the free-bound emission is simply  $\propto Q_{\text{H}}$ . The expressions are (Fernandez & Komatsu 2006)

$$L_{\nu}^{\text{ff,fb}} = 4\pi\gamma_{\text{c}}^{\text{ff,fb}} \frac{e^{-h_{\text{p}}\nu/kT}}{\sqrt{T}} \frac{Q_{\text{H}}}{\alpha_{\text{B}}(T)}, \quad (8)$$

where  $T$  is the temperature of the surrounding gas,  $k$  is the Boltzmann constant, and  $\alpha_{\text{B}}$  is the case B recombination coefficient (Seager et al. 1999). The expression of  $\gamma_{\text{c}}^{\text{ff,fb}}$  is given by Eq. (12) of Fernandez & Komatsu (2006).

Atoms at  $n = 2$  state is generated by both recombinations and collisional excitations, so the luminosity of two-photon emission is related to the rate of these two processes,

$$L_{\nu}^{\text{tp}} = \frac{2h_{\text{p}}\nu}{\nu_{\text{Ly}\alpha}} P(\nu/\nu_{\text{Ly}\alpha}) n_{\text{H}} V [f_{\text{e}}^2 \alpha_{\text{B}}(T) + f_{\text{e}}(1 - f_{\text{e}}) C_{\text{coll}}(T)], \quad (9)$$

where  $\nu_{\text{Ly}\alpha}$  is the frequency of Ly $\alpha$  photons,  $P(\nu/\nu_{\text{Ly}\alpha})$  is the normalized spectrum profile (Fernandez & Komatsu 2006),  $n_{\text{H}}$  is the number density of the Compton-thick material while  $V$  is the volume,  $f_{\text{e}}$  is the ionization fraction and  $C_{\text{coll}}(T)$  is the collisional excitation rate (Cantalupo et al. 2008). Considering the two constraints: the energy conversion  $\int (L_{\nu}^{\text{ff}} + L_{\nu}^{\text{fb}} + L_{\nu}^{\text{tp}} + L_{\nu}^{\text{abs}}) d\nu = L_{\text{Edd}}$  and the ionization equilibrium  $n_{\text{H}} V f_{\text{e}}^2 \alpha_{\text{B}}(T) = Q_{\text{H}}$ , to calculate the luminosity by Eqs. (8 & 9), we still need to know at least one of  $n_{\text{H}} V$ ,  $T$  and  $f_{\text{e}}$ . However, we find that with above two constraints, the final nebular emission is very insensitive to the  $f_{\text{e}}$ , so in all our calculations we assume  $f_{\text{e}}$  always equal to 0.5.

For  $M_{\text{BH}} = 10^6 M_{\odot}$  and  $N_{\text{H}} = 1.5 \times 10^{25} \text{ cm}^{-2}$ , we show the  $L_{\nu}^{\text{ff}}$ ,  $L_{\nu}^{\text{fb}}$ ,  $L_{\nu}^{\text{tp}}$  and  $L_{\nu}^{\text{abs}}$ , and the final emerging spectrum (their sum) in the bottom panel of Fig. 1. The  $L_{\nu}^{\text{em}}$  is the final spectrum we use for further calculations. In the presence of Compton-thick material, the radiation between  $\sim 3 - 10 \text{ eV}$ , which will be redshifted into the near infrared bands at present day, is boosted by a factor of  $\sim 10$ , while the emission in the X-ray bands is strongly suppressed. Similarly, UV photons  $> 13.6 \text{ eV}$  are completely absorbed so that these objects will not contribute to cosmic reionization.

## 2.2. NIRB and CXB fluctuations

The emissivity of a population of BHs formed at redshift  $z$  with initial mass  $M_{\text{BH,seed}}$  accreting at the Eddington rate for a time  $t_{\text{QSO}}$  and hosted in halos with virial temperature between  $10^4 \text{ K}$  and  $5 \times 10^4 \text{ K}$  is given by

$$\epsilon_{\nu}(z) = \frac{1}{4\pi} \int_{z_{\text{start}}}^z L_{\nu}^{\text{em}}(M') \frac{dn_{\text{BH}}}{dz'}(z') dz', \quad (10)$$

where  $M' = M_{\text{BH,seed}} \exp(t'/t_{\text{Edd}})$ ,  $t'$  is the time interval between  $z$  and  $z'$ ,  $t_{\text{Edd}} \approx 45 \text{ Myr}$  is the Eddington time scale (Salpeter 1964; Pelupessy et al. 2007). We assume that after the formation of a BH at redshift  $z'$ , the accretion only lasts for  $t_{\text{QSO}}$ , so it can only radiate when  $t' < t_{\text{QSO}}$ . We use a single typical value of  $M_{\text{BH,seed}}$  and  $t_{\text{QSO}}$  for all DCBHs. It is likely that the initial DCBH seeds span a mass range and are distributed according to a mass function  $f(M_{\text{seed}})$ . However, the DCBH spectrum in the UV band (contributing to the present-day NIRB) is almost independent of the BH mass. Therefore, the DCBH contribution can be well represented by an average mass  $\langle M_{\text{seed}} \rangle = \int M_{\text{seed}} f(M_{\text{seed}}) dM_{\text{seed}} / \int f(M_{\text{seed}}) dM_{\text{seed}}$ . In Eq. (10) the luminosity of a BH with mass  $M'$   $L_{\nu}^{\text{em}}(M') = 0$  when  $t' > t_{\text{QSO}}$ . The DCBH formation rate (per unit redshift) is

$$\frac{dn_{\text{BH}}}{dz'} = \int_{M_{\text{T4}}}^{M_{5\text{T4}}} f_{\text{p}}(M, z) \frac{d^2 n}{dz' dM} dM, \quad (11)$$

where  $dn/dM$  is the halo mass function (Sheth & Tormen 1999; Sheth et al. 2001) and  $M_{\text{T4}}$  and  $M_{5\text{T4}}$  are the halo masses corresponding to virial temperature  $10^4 \text{ K}$  and  $5 \times 10^4 \text{ K}$  respectively. We assume the DCBH formation can not take place in halos with virial temperature of  $T_{\text{vir}} \gtrsim 5 \times 10^4 \text{ K}$  for arguments given by Regan & Haehnelt (2009). The probability of a halo with mass  $M$  to be still metal-free at redshift  $z$ ,  $f_{\text{p}}$ , is taken from Schneider et al. (2006). As our redshift range is narrow, we neglect the evolution of  $f_{\text{p}}$  and use the results obtained for  $z = 15$ . We use the  $f_{\text{sn}} = 0.1$  model, see the red line of the upper right panel of Fig. 3 of Schneider et al. (2006). The value of  $f_{\text{p}}$  are (0.9, 0.7, 0.4) for halos with virial temperature of  $(1, 2, 5) \times 10^4 \text{ K}$ .

Assuming the source BHs are in the redshift range  $[z_{\text{start}}: z_{\text{end}}]$ , with above emissivity, the cumulative flux of the NIRB we receive on Earth is

$$\nu_0 I_{\nu_0} = \nu_0 \int_{z_{\text{start}}}^{z_{\text{end}}} \epsilon_{\nu}(z) \frac{dr_{\text{p}}}{dz} dz, \quad (12)$$

where  $r_p$  is the proper distance,  $\nu_0$  is the observed frequency,  $\nu = (1+z)\nu_0$ .

The contribution of accreting DCBHs to the angular power spectrum of the NIRB can be computed by considering only the two-halo correlation term, as each halo can host only one such object. The BH power spectrum is then

$$P_{\text{BH}}(k, z) \approx P(k, z)b_{\text{eff}}^2(z), \quad (13)$$

where

$$b_{\text{eff}}(z) = \frac{1}{\bar{n}_h} \int_{M_{\text{T4}}}^{M_{5\text{T4}}} b_h(M, z) \frac{dn}{dM} dM, \quad (14)$$

and  $b_h$  is the bias of halos with mass  $M$  relative to the matter fluctuations (Tinker et al. 2010) and  $\bar{n}_h$  is the mean number density of halos,

$$\bar{n}_h = \int_{M_{\text{T4}}}^{M_{5\text{T4}}} \frac{dn}{dM} dM. \quad (15)$$

The angular power spectrum of the NIRB from BHs in the redshift range  $[z_{\text{start}}: z_{\text{end}}]$  is (Cooray et al. 2012a)

$$C_l^{\text{NIRB}} = \int_{z_{\text{end}}}^{z_{\text{start}}} dz \frac{[\nu\epsilon_\nu(z)e^{-\tau(\nu_0, z)}]^2}{H(z)r^2(z)(1+z)^4} P_{\text{BH}}(z), \quad (16)$$

where  $r(z)$  is the comoving distance, and  $H(z)$  is the Hubble parameter. The optical depth  $\tau(\nu_0, z)$ , accounting for intergalactic absorption, is from Salvaterra & Ferrara (2003).

The same population, albeit Compton-thick, will also provide a contribution to CXB fluctuations. This can be computed with the above equations after replacing the term  $\nu\epsilon_\nu(z)e^{-\tau}$  with  $\int_{E_1(1+z)}^{E_2(1+z)} \epsilon_{E'}(z)dE'$  in Eq. (16). Here,  $E'$  is the energy of photons with frequency  $\nu'$ ,  $E_1$  and  $E_2$  are the energy values delimiting the observed X-ray band. We further assume that the IGM is transparent to X-rays (i.e.  $\tau(\nu_0, z) = 0$  for X-rays). Furthermore, DCBHs maybe sufficiently large to produce a detectable CXB-NIRB cross-correlation,

$$C_l^{\text{CXB-NIRB}} = \int_{z_{\text{end}}}^{z_{\text{start}}} dz \frac{[\nu\epsilon_\nu(z)e^{-\tau(\nu_0, z)} \int_{E_1(1+z)}^{E_2(1+z)} \epsilon_{E'}(z)dE']}{H(z)r^2(z)(1+z)^4} P_{\text{BH}}(z). \quad (17)$$

DCBHs will also contribute to the unresolved fraction of the CXB flux. The analogous for the X-ray background flux seen by an observer at redshift  $z = 0$  and energy  $E$  is given by

$$EJ(E) = E \int_{z_{\text{end}}}^{z_{\text{start}}} \epsilon_{E(1+z)}(z) \frac{dr_p}{dz} dz. \quad (18)$$

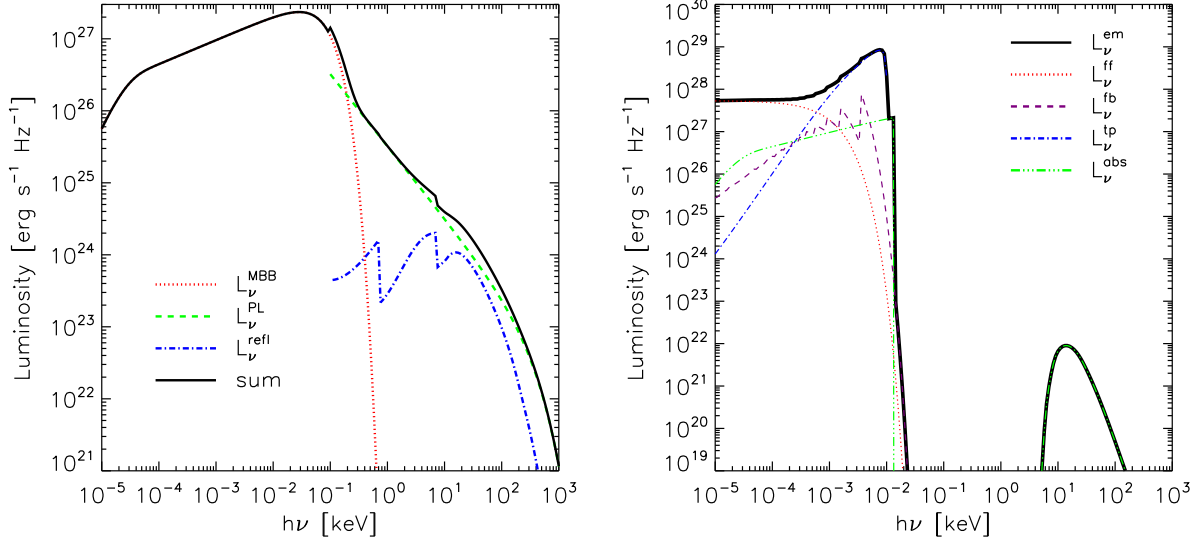


Fig. 1.— *Left*: the primary spectrum (solid) for a BH with  $M_{\text{BH}} = 10^6 M_{\odot}$  and its three components. *Right*: the emerging (thick solid line) quasar spectrum of above BH when  $N_{\text{H}} = 1.5 \times 10^{25} \text{ cm}^{-2}$  and the four components (thin lines).

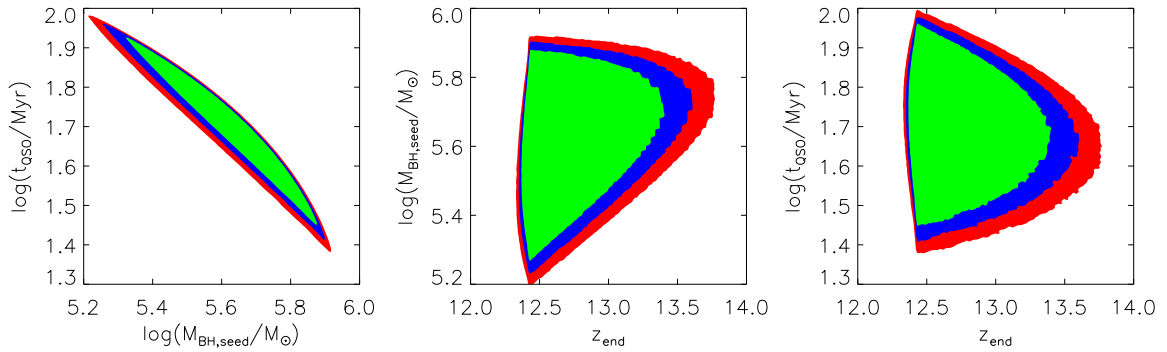


Fig. 2.— Constraints on the two dimensional parameters space of  $M_{\text{BH,seed}} - t_{\text{QSO}}$  (left),  $z_{\text{end}} - M_{\text{BH,seed}}$  (middle) and  $z_{\text{end}} - t_{\text{QSO}}$  (right). In each panel, regions filled by colors green, blue and red correspond to 1 - 3 $\sigma$  confidence level respectively.



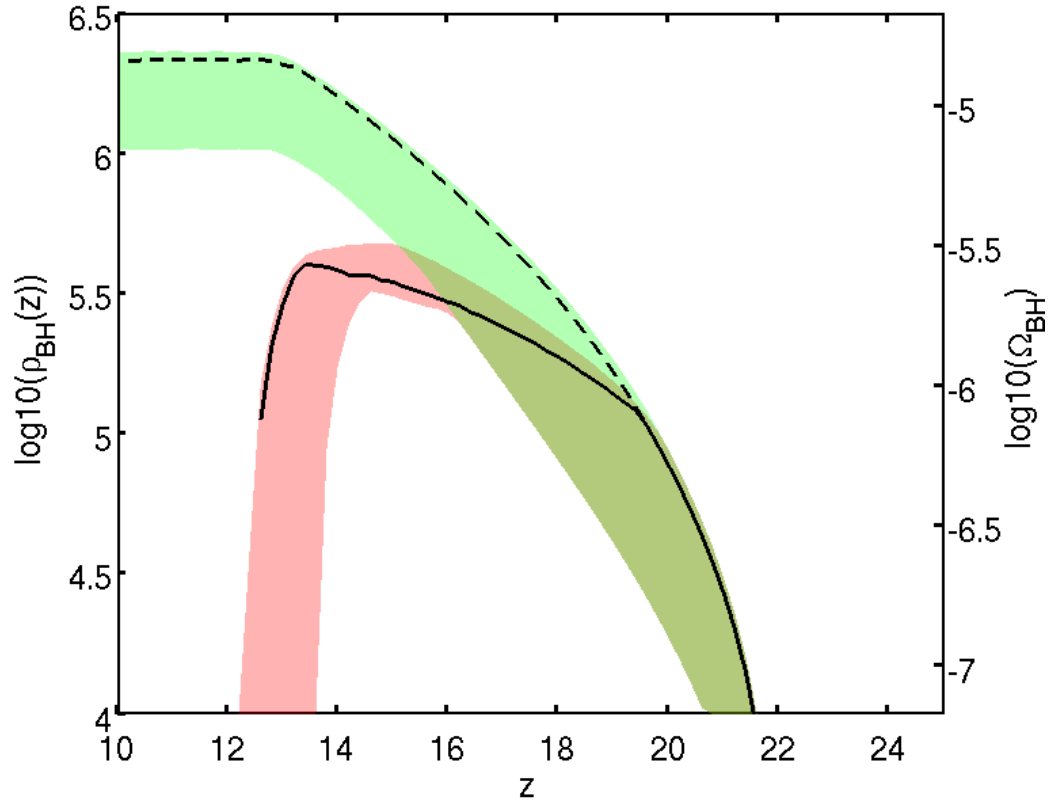


Fig. 3.— The cumulative mass density (in units of  $M_{\odot} \text{ Mpc}^{-3}$ ) of DCBHs (dashed) and the accreting ones (solid), only the latter contribute to the NIRB. Colored areas indicate regions corresponding to  $1\sigma$  dispersion around the mean values of  $(z_{\text{end}}, M_{\text{BH,seed}}, t_{\text{QSO}})$ . The right  $y$ -axis gives  $\Omega_{\text{BH}}$ , i.e.,  $\rho_{\text{BH}}/\rho_c$ , where  $\rho_c$  the critical density.

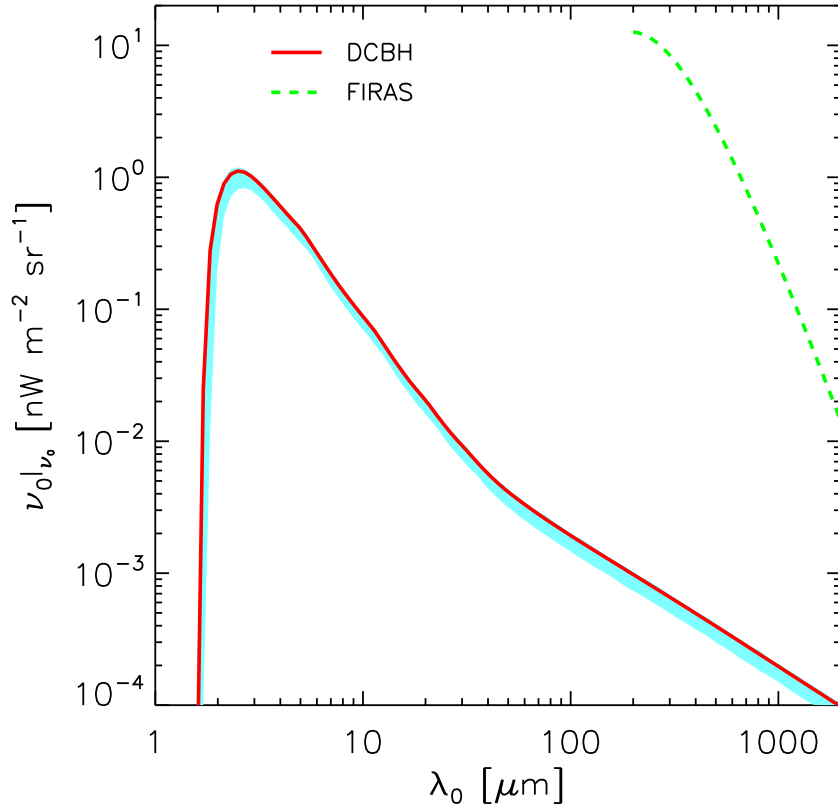


Fig. 4.— The contribution (solid) of DCBHs to the CIB with our best-fit parameters and the measured Cosmic Far-IR Background at 200-2000  $\mu\text{m}$  (dashed) fitted by Gispert et al. (2000). Colored areas indicate regions corresponding to  $1\sigma$  dispersion around the mean values of  $(z_{\text{end}}, M_{\text{BH,seed}}, t_{\text{QSO}})$ .

### 2.3. X-ray emission from undetected galaxies

In addition to high redshift DCBHs, it is necessary to include in the model also the contribution from low redshift galaxies to the X-ray flux. In fact, high-mass X-ray binaries (HMXBs) dominate the X-ray emission of normal star-forming galaxies (Mineo et al. 2012; Mirabel et al. 2011). Their cumulative X-ray luminosity is found to correlate linearly with the total (obscured and unobscured) star-formation rate (SFR) of the galaxy (Ranalli et al. 2003; Mineo et al. 2012), so that

$$L_{X,>0.5\text{keV}} \text{ (erg s}^{-1}\text{)} = 2.0 \times 10^{39} \text{SFR} (M_{\odot} \text{ yr}^{-1}). \quad (19)$$

We can estimate the SFR in the UV,  $\text{SFR}_{\text{UV}}^0$ , from the galaxy UV luminosity by (Iglesias-Páramo et al. 2006)

$$\text{SFR}_{\text{UV}}^0 (M_{\odot} \text{ yr}^{-1}) = 1.2 \times 10^{-43} L_{\text{UV,obs}} \text{ (erg s}^{-1}\text{)}, \quad (20)$$

where  $L_{\text{UV,obs}}$  is the observed cumulative UV luminosity at  $2312\text{\AA}$ . In order to derive the total SFR when dust obscuration is taken into account, we multiply  $\text{SFR}_{\text{UV}}^0$  by a factor of 5.2– the typical value for  $z \sim 2$  galaxies (Reddy et al. 2012) that dominate the small scale NIRB angular fluctuations and the shot noise level (Helgason et al. 2012). For an energy spectrum index 1.5,  $L_{X,0.5-8\text{keV}} = 0.75 L_{X,>0.5\text{keV}}$ , so the factor we used in Eq. (19) is  $\approx 60\%$  of the measurement of Mineo et al. (2012).

With above formula, we can compute the contribution of these faint galaxies to the CXB and the CXB-NIRB cross-correlation by adopting the galaxy number counts obtained in Helgason et al. (2012) and by simply replacing the near infrared flux of a galaxy with apparent magnitude  $m$  with its X-ray flux.

## 3. RESULTS

We compute the expected signal from a population of DCBHs formed at high redshift. As already discussed, DCBHs form only during a limited redshift range. Outside this range, the DCBH formation is unlikely: at earlier times bright LW sources are very rare, while later on the majority of atomic-cooling halos would have already been polluted by metals which induce a vigorous fragmentation (Schneider et al. 2002). In the following we will discuss the contribution of such DCBHs to the NIRB and to the CXB angular fluctuations.

### 3.1. NIRB fluctuations

We fit the NIRB fluctuation data (Cooray et al. 2012b) by minimizing the  $\chi^2$  with five free parameters, namely:  $z_{\text{start}}$ ,  $z_{\text{end}}$ , the mass of the DCBH seeds  $M_{\text{BH,seed}}$ , the accretion time scale  $t_{\text{QSO}}$ , and the hydrogen column density  $N_{\text{H}}$ . However, we find that the best-fit  $z_{\text{start}}$  should be  $\gtrsim 22$ , but our results are insensitive to the exact value of  $z_{\text{start}}$  as long as this is larger than  $z_{\text{start}} = 22$ ,

as sources at higher redshifts contribute only little to the NIRB. Therefore, in order to reduce the number of free parameters, we fix to  $z_{\text{start}} = 22$ . In addition, as long as  $N_{\text{H}} \gtrsim 10^{24} \text{ cm}^{-2}$ , the fit is also insensitive to this parameter, because for such high neutral hydrogen column density, the bulk of the emission  $> 13.6 \text{ eV}$  has already been re-processed to be nebular emission. We will show later on that a lower limit  $N_{\text{H}} > 1.2 - 1.3 \times 10^{25} \text{ cm}^{-2}$  is required not to exceed the CXB unresolved fraction. So in the following, we fix it to  $N_{\text{H}} = 1.5 \times 10^{25} \text{ cm}^{-2}$ .

The fit has been performed by minimizing the  $\chi^2$  over the three free parameters left and by requiring, as additional constraints, that the apparent magnitude of the single object should be  $> 30$  in the H-band of the HST/WFC3 and  $> 27$  in the 3.6 and 4.5  $\mu\text{m}$  band of Spitzer/IRAC. Since at scales  $\lesssim 100''$  the signal is dominated by the shot noise of low redshift, faint galaxies, the fit is performed to the large scale data only. We obtain the best-fit values and the one-parameter confidence interval:  $z_{\text{end}} = 12.44_{-0.07}^{+0.73}$ ,  $\log(M_{\text{BH,seed}}/M_{\odot}) = 5.85_{-0.40}^{+0.03}$  and  $\log(t_{\text{QSO}}/\text{Myr}) = 1.48_{-0.03}^{+0.34}$ , with a reduced  $\chi_r^2 = 0.9$ . A two-parameter confidence level study is presented in Fig. 2. As shown in the left panel, there is degeneracy between the mass of the BH seeds and  $t_{\text{QSO}}$ , as the contribution of a BH to the emissivity is approximately  $\propto M_{\text{BH,seed}}(e^{t_{\text{QSO}}/t_{\text{Edd}}} - 1)$ . Even considering the redshift dependence, this degeneracy cannot be broken by using NIRB observations only. The sharp cut-off on  $z_{\text{end}}$  at  $\sim 12.4$  present in the contour plots comes from the assumption that individual DCBHs are not detected by current instruments, and, in particular, by the fact that they should be fainter than  $m = 30$  in the H-band of the HST/WFC3. The sharp cut-off could be the result of our simplified assumptions on a typical value of the seed mass and  $t_{\text{QSO}}$  and that a more realistic model can result in a more gentle decline of  $\rho_{\text{BH}}$  at  $z < 12.4$ .

With above best-fit parameters, we calculate the density of all mass locked in BHs form through direct collapse, and the density of DCBHs which are accreting at the corresponding redshift by

$$\rho_{\text{BH}}(z) = \int_z^{z_{\text{start}}} M' \frac{dn_{\text{BH}}}{dz'} dz', \quad (21)$$

when  $t' < t_{\text{QSO}}$ ,  $M' = M_{\text{BH,seed}} \exp(t'/t_{\text{Edd}})$ ; when  $t' > t_{\text{QSO}}$ ,  $M' = M_{\text{BH,seed}} \exp(t_{\text{QSO}}/t_{\text{Edd}})$  for density of all DCBHs, while  $M' = 0$  for accreting DCBHs. We plot these two densities (and the BH density parameter  $\Omega_{\text{BH}}$  on right  $y$ -axis) in Fig. 3. The shaded regions correspond to the  $1\sigma$  uncertainty on the model free parameters. Note that the upper limit of the uncertainty regions is also limited by our assumption that each BH is undetected in current surveys. The surface density of the accreting DCBHs is  $7.7 \times 10^6 \text{ deg}^{-2}$  and their magnitudes at 3.6 and 4.5  $\mu\text{m}$  are below the current detection limit of *Spitzer*.

The contribution of DCBHs to the background intensity, computed by Eq. (12), is shown in Fig. 4; the shaded region represent the  $1\sigma$  uncertainty on the model free paramters. In the NIR bands this is about an order on magnitude below the one of ordinary low- $z$  galaxies (Helgason et al. 2012) but higher than the predicted signal of  $z > 6$  galaxies (Yue et al. 2013). At 3.6 and 4.5  $\mu\text{m}$  bands DCBHs provide an intensity of 0.7 and 0.5  $\text{nW m}^{-2} \text{ s}^{-1}$ , respectively. The total contribution of undetected sources (galaxies plus DCBHs) is still consistent with available measures and limits on the unresolved NIRB fraction. At longer wavelengths, the DCBH contribution declines rapidly to a

value  $> 100$  times smaller than the Cosmic Far-IR Background measured by FIRAS (Gispert et al. 2000).

We show the NIRB fluctuations produced by the population of high redshift DCBHs in Fig. 5 (dashed line). We also plot the contribution from low redshift ( $z < 5$ ) faint galaxies (dash-dotted-dotted) by following the reconstruction of Helgason et al. (2012), and the contribution from high redshift ( $z > 5$ ) galaxies studied in Yue et al. (2013) (dash-dotted lines). The solid line is their sum, while the shaded regions represent the range of  $1\sigma$  goodness-of-fit. Points with errorbars are measurements presented in Cooray et al. (2012b). In the theoretical calculation we remove the galaxies brighter than  $m = 24$  to match the model shot noise level to the observed values. As clearly seen in Fig. 5, faint galaxies (including both the high redshift and low redshift ones) are unable to provide the observed source-subtracted NIRB fluctuations at large scales, which can be instead explained by the accreting DCBHs.

### 3.2. CXB fluctuations and cross-correlation

Albeit Compton-thick, DCBH may still contribute to the unresolved fraction of the CXB and to its spatial fluctuations. For the best-fit parameters of our model presented previously, we try to vary the adopted value of the hydrogen column density. We find that  $N_{\text{H}} > 1.2 - 1.3 \times 10^{25} \text{ cm}^{-2}$  is required (see Fig. 6 where the CXB flux as a function of  $N_{\text{H}}$  is shown) not to exceed available limits (Moretti et al. 2012), further supporting our assumption of Compton-thick accretion. We note that this also reduces the tension between the need for an efficient and rapid growth of BH seeds into the SMBHs powering quasar activity at  $z = 6 - 7$  and the strict upper limit on the global accreted mass deduced from X-ray background observations (Salvaterra et al. 2012).

We also show the contribution to the angular power spectrum of the CXB from DCBHs in the left panel of Fig. 7, when  $N_{\text{H}}$  is set to be  $1.5 \times 10^{25} \text{ cm}^{-2}$ , together with the contributions from other components modeled in Cappelluti et al. (2012b), and the latest measurements in the same paper. The contribution of DCBHs to CXB fluctuations is found to be negligible with respect the other sources at all angular scales.

As DCBHs contribute to both the NIRB and the CXB, it is natural to expect a CXB-NIRB cross-correlation signal (dashed line in the right panel of Fig. 7). For  $N_{\text{H}} = 1.5 \times 10^{25} \text{ cm}^{-2}$  the expected CXB (0.5-2 keV)-NIRB ( $4.5\mu\text{m}$ ) cross-correlation signal is  $\simeq 8 \times 10^{-12} \text{ erg s}^{-1} \text{ cm}^{-2} \text{ nW m}^{-2} \text{ sr}^{-1}$  at scales  $\theta > 100''$ , as indeed tentatively reported by Cappelluti et al. (2012a). At lower scales, the CXB-NIRB is dominated by undetected low- $z$  galaxies (dashed-dotted line). This has been computed as discussed in Section 2.3 adopting a limiting magnitude  $\approx 25$  to let the model predicted shot noise level of the NIRB match the observation (Kashlinsky et al. 2012; Cappelluti et al. 2012a). We also check that the corresponding X-ray flux is below the point source

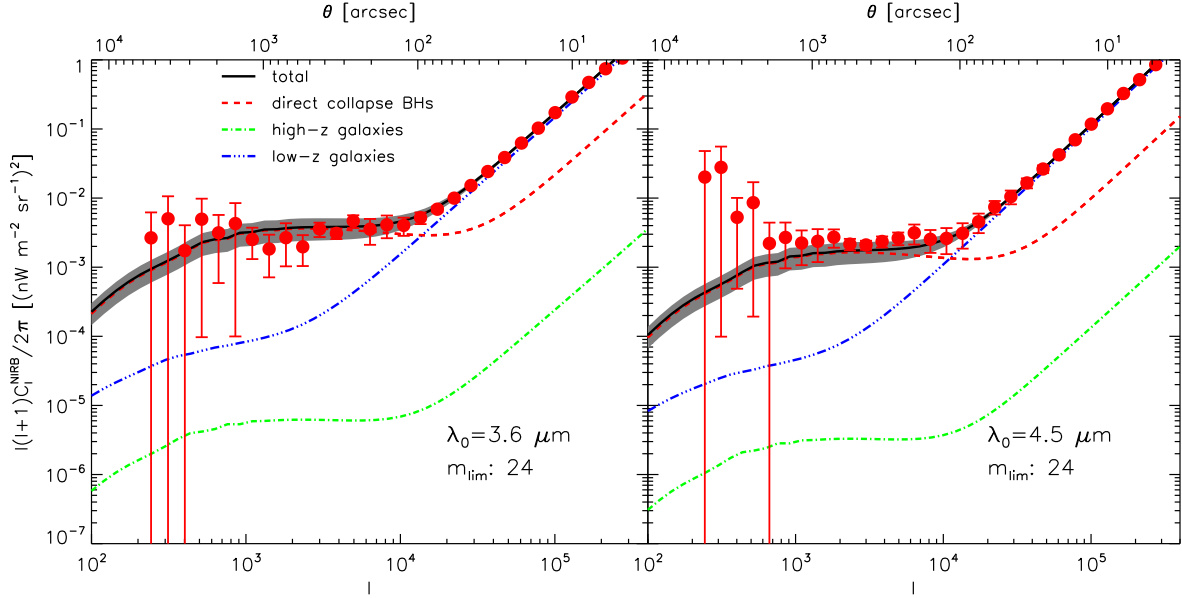


Fig. 5.— NIRB angular power spectrum at wavelength  $3.6 \mu\text{m}$  (left) and  $4.5 \mu\text{m}$  (right), with the contribution from different sources: (a) accreting DCBH (dashed line); (b) high redshift ( $z > 5$ ) faint galaxies with  $m > 24$  (dot-dashed); (c) low redshift faint galaxies ( $z < 5$  and  $m > 24$ , dot-dot-dot-dashed) from Helgason et al. (2012). The solid line is the total with the shaded area marking the  $1\sigma$  goodness-of-fit. Galaxy contributions are taken from Yue et al. (2013). The points are the latest measurements from Cooray et al. (2012b). The DCBH term accounts for the large scale (typically  $> 100''$ ) clustering signal of the fluctuation spectra; at smaller scales shot noise, i.e., Poisson fluctuations of source number counts in the beam, dominates.

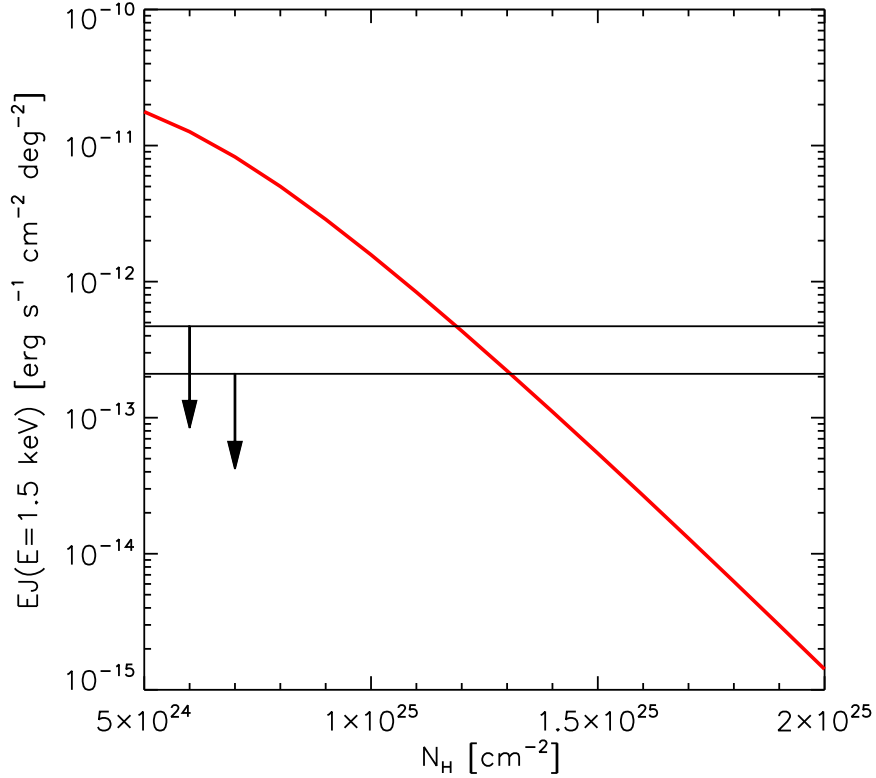


Fig. 6.— Contribution of DCBHs to the CXB flux at 1.5 keV as a function of  $N_{\text{H}}$ . The two horizontal lines (marked by arrows) refer to the recent upper limits to the unresolved fraction by Moretti et al. (2012): upper line is the maximum value allowed by the data ( $0.47 \times 10^{-12} \text{ erg s}^{-1} \text{ cm}^{-2} \text{ deg}^{-2}$ ), while the lower one ( $0.21 \times 10^{-12} \text{ erg s}^{-1} \text{ cm}^{-2} \text{ deg}^{-2}$ ) is the more stringent limit obtained by subtracting the contributions of the low redshift AGNs modeled by Gilli et al. (2007). Hydrogen column densities  $> 1.2 - 1.3 \times 10^{25} \text{ cm}^{-2}$  are required to not exceed the observational limits.

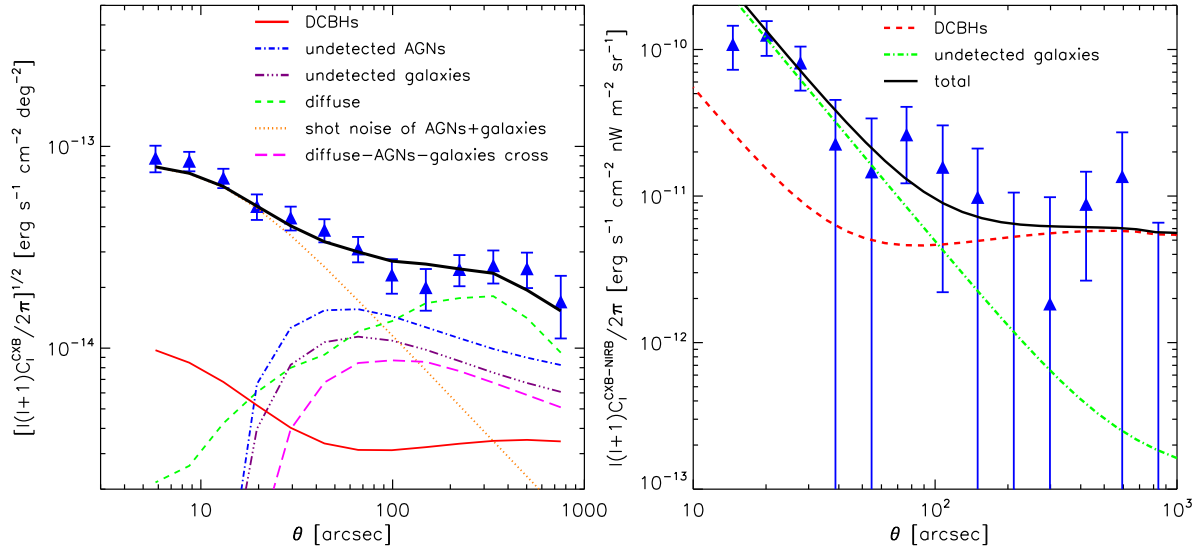


Fig. 7.— *Left panel:* Angular power spectrum of the CXB between 0.5-2.0 keV showing contribution from different sources: DCBHs (solid), undetected AGNs (dot-dashed), X-ray undetected galaxies (dot-dot-dot-dashed), hot intergalactic medium (short-dashed), shot noise of AGNs and galaxies (dotted). The solid thick line is the sum of different components. The data (triangles) and all curves except from the DCBHs are from Cappelluti et al. (2012b). *Right panel:* CXB (0.5-2.0 keV)-NIRB(4.5  $\mu\text{m}$ ) cross-correlation power spectrum. The predicted signal from DCBHs is shown with the dashed line for  $N_{\text{H}} = 1.5 \times 10^{25} \text{ cm}^{-2}$ , while the contribution from faint X-ray emitting galaxies is shown with dash-dotted line, the solid line is the sum. Data points are from Cappelluti et al. (2012a).



flux limit of Cappelluti et al. (2012a) observations<sup>2</sup>.

In conclusion, the observed CXB-NIRB cross-correlation can be explained by a combination of X-ray emission from HMXBs in faint, low- $z$  galaxies at small angular scales and the DCBH contribution at large scales. We note that at very small scales, i.e.,  $\theta \lesssim 20''$ , the observed cross-correlation drops. This is likely due to the instrument PSF of the X-ray observation, and (possibly) beam effects in NIRB observations, not modeled here. The analogous cross-correlation for the CXB 2-7 keV band is found to be negligible, in agreement with the findings of Cappelluti et al. (2012a).

#### 4. CONCLUSIONS

We studied the spectrum of accreting black holes formed through the direct collapse of metal-free gas in halos with virial temperature  $\gtrsim 10^4$  K. BHs formed by this process are very likely to be Compton-thick, so that: (a) as most of photons with  $h\nu > 13.6$  eV are absorbed by the large column density of surrounding gas, the contribution of these objects to reionization is negligible and that to the CXB is reduced significantly; (b) ionizing photons are re-processed into optical-UV photons (free-free, free-bound and two-photon emission) while Ly $\alpha$  photons are trapped and finally converted into two-photon emission. These secondary photons eventually escape the object and considerably boost (by a factor  $\sim 10$ ) the contribution of these sources to the NIRB.

We calculated the contribution of DCBHs to the NIRB fluctuations, by fitting the latest observations at 3.6 and 4.5  $\mu\text{m}$ . We find that observed fluctuations at angular scales larger than  $\theta = 100''$  can be explained by DCBHs formed in metal-free halos with virial temperature  $T_{\text{vir}} = 1 - 5 \times 10^4$  K down to  $z_{\text{end}} = 12.44_{-0.07}^{+0.73}$ , with initial masses  $\log(M_{\text{BH,seed}}/M_{\odot}) = 5.85_{-0.40}^{+0.03}$  and accreting gas at the Eddington limit for a time  $\log(t_{\text{QSO}}/\text{Myr}) = 1.48_{-0.03}^{+0.34}$ .

Using the above best-fit parameters, we have calculated the DCBH contribution to the CXB intensity at 1.5 keV, finding it well below the current observational limits as long as the sources are Compton-thick with  $N_{\text{H}} > 1.2 - 1.3 \times 10^{25} \text{ cm}^{-2}$ . Analogously, DCBHs contribute only little to the CXB angular power spectrum.

However, we predict that the DCBHs signal could emerge in the CXB-NIRB cross-correlation at scales  $> 100''$ . For  $N_{\text{H}} = 1.5 \times 10^{25} \text{ cm}^{-2}$  the cross-correlation level of the DCBH population is  $\simeq 8 \times 10^{-12} \text{ erg s}^{-1} \text{ cm}^{-2} \text{ nW m}^{-2} \text{ sr}^{-1}$ , in good agreement with recent observations, despite the remaining large uncertainties in current data. In addition, we also found that the observed cross-correlation signal at small scales ( $< 100''$ ) can be explained by the HMXBs hosted in faint, low- $z$  galaxies also dominating the small scale NIRB angular fluctuations.

---

<sup>2</sup>We note that the cross-correlation signal decreases for larger obscuring column densities; thus, in principle, the CXB-NIRB cross-correlation can be used to obtain a more accurate determination of  $N_{\text{H}}$  once more precise data will become available.

Thus, the NIRB fluctuations and their cross-correlation with the CXB might be the smoking gun of a peculiar population of early intermediate mass BHs; they might also shed light on the challenging questions posed by the rapid formation of SMBHs seen in quasars.

### ACKNOWLEDGMENTS

It is a pleasure to acknowledge intense discussions and data exchange with N. Cappelluti, A. Cooray, K. Helgason, E. Komatsu, T. Matsumoto, R. Thompson, S. Kashlinsky, S. Mitra and T. Choudhury. We acknowledge financial support from PRIN MIUR 2010-2011, project “The Chemical and Dynamical Evolution of the Milky Way and Local Group Galaxies”, prot. 2010LY5N2T. AF thanks UT Austin for support and hospitality as a Centennial B. Tinsley Professor and the stimulating atmosphere of the NIRB Workshop organized by the Texas Cosmology Center. BY thanks support and hospitality by SNS through the Distinguished Visiting Program. BY and XC also acknowledges the support of the NSFC grant 11073024 and the MoST Project 863 grant 2012AA121701. YX is supported by China Postdoctoral Science Foundation and by the Young Researcher Grant of National Astronomical Observatories, Chinese Academy of Sciences.

### REFERENCES

- Abel T., Anninos P., Zhang Y., Norman M. L., 1997, *New A*, 2, 181
- Agarwal B., Khochfar S., Johnson J. L., Neistein E., Dalla Vecchia C., Livio M., 2012, *MNRAS*, 425, 2854
- Alvarez M. A., Wise J. H., Abel T., 2009, *ApJ*, 701, L133
- Balucinska-Church M., McCammon D., 1992, *ApJ*, 400, 699
- Begelman M. C., Volonteri M., Rees M. J., 2006, *MNRAS*, 370, 289
- Bromm V., Loeb A., 2003, *ApJ*, 596, 34
- Brown R. L., Mathews W. G., 1970, *ApJ*, 160, 939
- Burigana C., 1995, *MNRAS*, 272, 481
- Cantalupo S., Porciani C., Lilly S. J., 2008, *ApJ*, 672, 48
- Cappelluti N. et al., 2012a, ArXiv e-prints, arXiv:1210.5302
- Cappelluti N. et al., 2012b, *MNRAS*, 427, 651
- Chen X., Kamionkowski M., 2004, *Phys. Rev. D*, 70, 043502

- Cooray A., Bock J. J., Keatin B., Lange A. E., Matsumoto T., 2004, *ApJ*, 606, 611
- Cooray A., Gong Y., Smidt J., Santos M. G., 2012a, *ApJ*, 756, 92
- Cooray A. et al., 2012b, *Nature*, 490, 514
- Cooray A., Yoshida N., 2004, *MNRAS*, 351, L71
- Dijkstra M., Haiman Z., Mesinger A., Wyithe J. S. B., 2008, *MNRAS*, 391, 1961
- Draine B. T., Bertoldi F., 1996, *ApJ*, 468, 269
- Eisenstein D. J., Hu W., 1998, *ApJ*, 496, 605
- Fan X. et al., 2001, *AJ*, 122, 2833
- Fernandez E. R., Komatsu E., 2006, *ApJ*, 646, 703
- Fiocchi M., Bazzano A., Ubertini P., Zdziarski A. A., 2007, *ApJ*, 657, 448
- Gilli R., Comastri A., Hasinger G., 2007, *A&A*, 463, 79
- Gispert R., Lagache G., Puget J. L., 2000, *A&A*, 360, 1
- Haiman Z., Abel T., Rees M. J., 2000, *ApJ*, 534, 11
- Helgason K., Ricotti M., Kashlinsky A., 2012, *ApJ*, 752, 113
- Iglesias-Páramo J. et al., 2006, *ApJS*, 164, 38
- Johnson J. L., Whalen D. J., Fryer C. L., Li H., 2012a, *ApJ*, 750, 66
- Johnson J. L., Whalen D. J., Li H., Holz D. E., 2012b, *ArXiv e-prints arXiv:1211.0548*
- Kashlinsky A., Arendt R., Gardner J. P., Mather J. C., Moseley S. H., 2004, *ApJ*, 608, 1
- Kashlinsky A., Arendt R. G., Ashby M. L. N., Fazio G. G., Mather J., Moseley S. H., 2012, *ApJ*, 753, 63
- Kashlinsky A., Arendt R. G., Mather J., Moseley S. H., 2005, *Nature*, 438, 45
- Kashlinsky A., Arendt R. G., Mather J., Moseley S. H., 2007, *ApJ*, 654, L5
- Kashlinsky A., Odenwald S., Mather J., Skrutskie M. F., Cutri R. M., 2002, *ApJ*, 579, L53
- Koushiappas S. M., Bullock J. S., Dekel A., 2004, *MNRAS*, 354, 292
- Kuhlen M., Madau P., 2005, *MNRAS*, 363, 1069
- Lacey C., Cole S., 1993, *MNRAS*, 262, 627

- Latif M. A., Zaroubi S., Spaans M., 2011, MNRAS, 411, 1659
- Lodato G., Natarajan P., 2006, MNRAS, 371, 1813
- Machacek M. E., Bryan G. L., Abel T., 2001, ApJ, 548, 509
- Madau P., Rees M. J., Volonteri M., Haardt F., Oh S. P., 2004, ApJ, 604, 484
- Magdziarz P., Zdziarski A. A., 1995, MNRAS, 273, 837
- Makishima K. et al., 2000, ApJ, 535, 632
- Matsumoto T. et al., 2011, ApJ, 742, 124
- McQuinn M., Lidz A., Zaldarriaga M., Hernquist L., Hopkins P. F., Dutta S., Faucher-Giguère C.-A., 2009, ApJ, 694, 842
- Miller M. C., Colbert E. J. M., 2004, International Journal of Modern Physics D, 13, 1
- Mineo S., Gilfanov M., Sunyaev R., 2012, MNRAS, 419, 2095
- Mirabel I. F., Dijkstra M., Laurent P., Loeb A., Pritchard J. R., 2011, A&A, 528, A149
- Miralda-Escudé J., 2003, Science, 300, 1904
- Mitsuda K. et al., 1984, PASJ, 36, 741
- Mo H. J., White S. D. M., 1996, MNRAS, 282, 347
- Moretti A., Vattakunnel S., Tozzi P., Salvaterra R., Severgnini P., Fugazza D., Haardt F., Gilli R., 2012, A&A, 548, A87
- Murphy K. D., Yaqoob T., 2009, MNRAS, 397, 1549
- Omukai K., 2001, ApJ, 546, 635
- O’Shea B. W., Norman M. L., 2008, ApJ, 673, 14
- Park K., Ricotti M., 2011, ApJ, 739, 2
- Pelupessy F. I., Di Matteo T., Ciardi B., 2007, ApJ, 665, 107
- Petri A., Ferrara A., Salvaterra R., 2012, MNRAS, 422, 1690
- Ranalli P., Comastri A., Setti G., 2003, A&A, 399, 39
- Reddy N. et al., 2012, ApJ, 744, 154
- Regan J. A., Haehnelt M. G., 2009, MNRAS, 396, 343

- Salpeter E. E., 1964, *ApJ*, 140, 796
- Salvaterra R., Ferrara A., 2003, *MNRAS*, 339, 973
- Salvaterra R., Ferrara A., 2006, *MNRAS*, 367, L11
- Salvaterra R., Ferrara A., Dayal P., 2011, *MNRAS*, 414, 847
- Salvaterra R., Haardt F., Ferrara A., 2005, *MNRAS*, 362, L50
- Salvaterra R., Haardt F., Volonteri M., Moretti A., 2012, *A&A*, 545, L6
- Santos M. R., Bromm V., Kamionkowski M., 2002, *MNRAS*, 336, 1082
- Sazonov S. Y., Ostriker J. P., Sunyaev R. A., 2004, *MNRAS*, 347, 144
- Schleicher D. R. G., Spaans M., Glover S. C. O., 2010, *ApJ*, 712, L69
- Schneider R., Ferrara A., Natarajan P., Omukai K., 2002, *ApJ*, 571, 30
- Schneider R., Salvaterra R., Ferrara A., Ciardi B., 2006, *MNRAS*, 369, 825
- Seager S., Sasselov D. D., Scott D., 1999, *ApJ*, 523, L1
- Shang C., Bryan G. L., Haiman Z., 2010, *MNRAS*, 402, 1249
- Sheth R. K., Mo H. J., Tormen G., 2001, *MNRAS*, 323, 1
- Sheth R. K., Tormen G., 1999, *MNRAS*, 308, 119
- Sheth R. K., Tormen G., 2002, *MNRAS*, 329, 61
- Shibata M., Shapiro S. L., 2002, *ApJ*, 572, L39
- Spaans M., Silk J., 2006, *ApJ*, 652, 902
- Tegmark M., Silk J., Rees M. J., Blanchard A., Abel T., Palla F., 1997, *ApJ*, 474, 1
- Thompson R. I., Eisenstein D., Fan X., Rieke M., Kennicutt R. C., 2007, *ApJ*, 657, 669
- Tinker J. L., Robertson B. E., Kravtsov A. V., Klypin A., Warren M. S., Yepes G., Gottlöber S., 2010, *ApJ*, 724, 878
- Valdés M., Ferrara A., 2008, *MNRAS*, 387, L8
- Volonteri M., Lodato G., Natarajan P., 2008, *MNRAS*, 383, 1079
- Volonteri M., Rees M. J., 2005, *ApJ*, 633, 624
- Wolcott-Green J., Haiman Z., Bryan G. L., 2011, *MNRAS*, 418, 838

Xu Y., Ferrara A., Chen X., 2011, MNRAS, 410, 2025

Yaqoob T., 1997, ApJ, 479, 184 (Y97)

Yue B., Ferrara A., Salvaterra R., Chen X., 2013, MNRAS, 431, 383

Zhang J., Hui L., 2006, ApJ, 641, 641

### A. Conditions for BH formation by direct collapse

The key factor for the formation of a BH by direct collapse is the destruction of  $\text{H}_2$  molecules to prevent gas fragmentation. This is possible when the halo is immersed in a strong radiation field that either directly photo-dissociates  $\text{H}_2$  molecules via UV LW photons (Machacek et al. 2001; O’Shea & Norman 2008), or photo-detaches  $\text{H}^-$ , the critical intermediate species for the  $\text{H}_2$  formation channel (Tegmark et al. 1997; Abel et al. 1997), by photons with energies  $\gtrsim 0.76$  eV (Shang et al. 2010). Relatively high values of the radiation field intensity are required in order for  $\text{H}_2$  suppression to be effective, since for high gas densities self-shielding effects (Haiman et al. 2000; Draine & Bertoldi 1996; Wolcott-Green et al. 2011) can protect  $\text{H}_2$ . Therefore, at early times, the formation of DCBHs relies on local fluctuations of the radiation field and it is possible only in biased regions where the background intensity from nearby sources is sufficiently large<sup>3</sup>. Once a massive BH eventually formed, it will also act as an additional source of UV photons, thus inducing a positive feedback. We assume the DCBH formation can not take place in halos with virial temperature of  $T_{\text{vir}} \gtrsim 5 \times 10^4$  K for arguments given by Regan & Haehnelt (2009).

At  $z = 15$  the intensity of the radiation of an accreting BH with mass  $10^6 M_{\odot}$  at 12.87 eV drops below  $50 \times 10^{-21} \text{ erg s}^{-1} \text{ cm}^{-2} \text{ Hz}^{-1} \text{ sr}^{-1}$  at a distance  $r \approx 90$  kpc (comoving). Assuming that this radiation field is sufficient to suppress  $\text{H}_2$  formation (the threshold value might depend on the detailed spectral shape, see below), the formation of another BH by direct collapse is possible in halos with  $10^4 \text{ K} \lesssim T_{\text{vir}} \lesssim 5 \times 10^4 \text{ K}$  hosted in a region between about two virial radii of the first halo and  $r$ . The number of neighbors in this region can be computed from the two-point correlation function  $\xi(r, z)$ ,

$$N_{\text{neig}}(z) = \bar{n}_h \int_{r_{\text{min}}}^{r_{\text{max}}} [1 + \xi(r, z)] 4\pi r^2 dr. \quad (\text{A1})$$

The two-point correlation function for a region of mass  $M_1$  and linear overdensity  $\delta_1$  is

$$\xi(r, z) = \frac{1}{2\pi^2} \int P_{1,\text{BH}}(k, z) \frac{\sin(kr)}{kr} k^2 dk, \quad (\text{A2})$$

---

This preprint was prepared with the AAS L<sup>A</sup>T<sub>E</sub>X macros v5.2.

<sup>3</sup>This situation has been investigated by Dijkstra et al. (2008) and Agarwal et al. (2012) who discussed the case in which the LW is produced by a combination of normal galaxies and Pop III stars. They conclude that the DCBH formation rate is modest. For example, Agarwal et al. (2012) gives  $\sim 10^{-3} - 10^{-2} \text{ Mpc}^{-3} z^{-1}$ . Their results do not conflict with our discussion because in their model radiation from DCBHs themselves was not included.

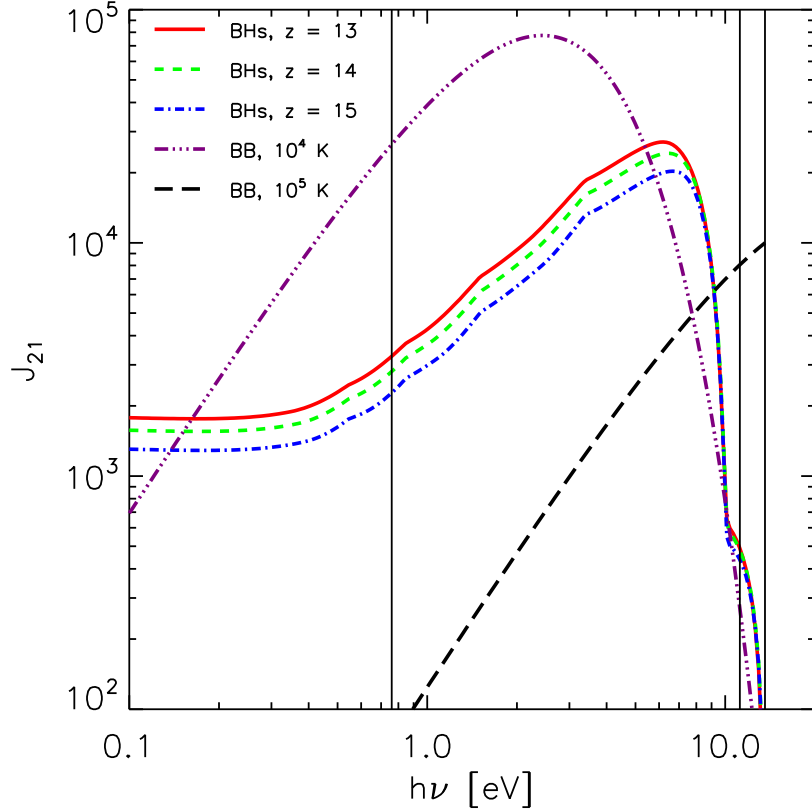


Fig. 8.— The background radiation field from the population of accreting DCBHs between 0.1 eV and 13.6 eV computed at  $z = 13, 14, 15$  and shown with the solid, dashed, dot-dashed lines, respectively. We also show the critical spectrum for the formation of DCBHs from Shang et al. (2010) corresponding to black body temperature  $10^4$  K and  $10^5$  K.  $J_{21}$  is the special intensity in units of  $10^{-21}$  erg s $^{-1}$  cm $^{-2}$  Hz $^{-1}$  sr $^{-1}$ . For the former  $J_{21} = 30$  at 13.6 eV, while for the latter  $J_{21} = 10^4$  at 13.6 eV. By thin vertical lines, we mark  $h\nu = 0.76$  eV, above which the  $\text{H}^-$  dissociation is possible, and the interval  $h\nu = 11.2$  eV – 13.6 eV, i.e., the LW radiation range.

where  $P_{1,\text{BH}}(k, z)$  is the power spectrum of the spatial fluctuations of BHs in this region. This is computed as  $P_{1,\text{BH}}(k, z) = P(k, z)b_{1,\text{eff}}^2(z)$ , where  $P(k, z)$  is the mean cosmic matter power spectrum; the bias for this region,  $b_{1,\text{eff}}(z)$ , is derived from Eq. (14) by replacing  $dn/dM$  with the mass function of halos in the given region  $M_1$ , as computed by the Extended Press-Schechter theory (Lacey & Cole 1993; Mo & White 1996; Sheth & Tormen 2002).

The above argument can be expressed in terms of a critical linear overdensity  $\delta_c$  for which one neighbor is within the influence radius  $r$  of the halo hosting the accreting BH. Regions with  $\delta_1 > \delta_c$  have one or more neighbors and the BH can promote further BH formation by direct collapse in these halos. The distribution of regions above the critical overdensity as a function of  $M_1$  can be determined by the distribution of distances that random walks have traveled before first up-crossing the density barrier, and can be computed by using the method proposed by Zhang & Hui (2006). We find that at  $z = 15$  in about 20% of the cosmic volume, halos with  $10^4 \text{ K} \lesssim T_{\text{vir}} \lesssim 5 \times 10^4 \text{ K}$  have on average at least one neighbor in the same mass range within a radius of  $\leq 90 \text{ kpc}$ .

The formation of the first DCBH must be triggered by the UV background produced by normal or Population III star forming galaxies. However, the collective radiation from newly formed BHs adds to this background and further increases it. In Fig. 8 we show the BH specific background intensity  $J(\nu)$  at frequency  $\nu$  using the emissivity  $\epsilon_\nu(z)$  predicted by our model and computed using the following expression:

$$J(\nu, z) = (1 + z)^3 \int_z^{z_{\text{start}}} \epsilon_{\nu'}(z') e^{-\tau} \frac{dr_p}{dz'} dz', \quad (\text{A3})$$

where  $\nu' = \nu(1 + z)/(1 + z')$ , and  $r_p$  is the proper distance. The precise  $\text{H}_2$  suppression intensity threshold for this specific spectral shape is unavailable as previous studies have only explored black-body (stellar) spectra of temperatures of  $10^4 \text{ K}$  and  $10^5 \text{ K}$  (Shang et al. 2010), or a power law form spectrum (Omukai 2001). The critical curves for these two black-body cases are also reported in Fig. 8 as a function of energy.

In the LW regime, our background radiation is weaker than the  $10^5 \text{ K}$  black body critical spectrum, but higher than the  $10^4 \text{ K}$  one. On the other hand, for energies  $\gtrsim 0.76 \text{ eV}$ , radiation from accreting DCBHs is much larger than the  $10^5 \text{ K}$  critical case, yet lower than the  $10^4 \text{ K}$  one. Thus, our spectrum is somewhat “intermediate” between those studied by Shang et al. (2010). Lacking specific numerical simulations, it is presently hard to quantify the exact intensity threshold value; the previous results can only provide a consistency check.

## B. Photoelectric absorption and Compton scattering

In this Appendix, we briefly summarize the formulae derived by Y97 and used here to calculate the absorbed and scattered spectrum of a BH. This emerging spectrum is the sum of the unabsorbed primary spectrum and the flux from all scattering orders:



$$N(E) = N_i(E)e^{-\tau_0} + \sum_1^{n_{\max}} N_n(E), \quad (\text{B1})$$

where  $N(E)$  is the emerging photon number flux at energy  $E$ ,  $N_i(E)$  is the primary spectrum (corresponding to the solid line in the upper panel of Fig. 1), while  $N_n(E)$  is the flux of photons that have already been scattered exactly  $n$  ( $n \leq n_{\max}$ ) times and then escape the medium. We use  $n_{\max} = 20$  after checking convergence of the results for  $N_H$  considered in this work. The optical depth  $\tau_0$  is the sum of scattering optical depth and the photoelectric absorption optical depth,

$$\tau_0 = \tau_s + \sigma_{\text{abs}}(E)N_H = [1.2\sigma_T + \sigma_{\text{abs}}(E)]N_H, \quad (\text{B2})$$

where  $\sigma_T = 0.67 \times 10^{-24} \text{ cm}^{-2}$  is the cross-section of Thomson scattering.  $\sigma_{\text{abs}}(E)$  is the cross-section of photon ionization, when  $0.03 \text{ keV} < E < 10 \text{ keV}$ , the data is fitted by Balucinska-Church & McCammon (1992); for  $E > 10 \text{ keV}$ , we get this cross-section by the extrapolation of a  $\propto E^{-3}$  law.

To get the final expression for  $N_n(E)$  we proceed as follows. The fraction of photons with initial energy  $E_0$  that have never been absorbed or scattered by the medium is  $P_0 = e^{-\tau_0}$ , so that a fraction  $1 - P_0$  of them is either absorbed or scattered. Suppose a fraction  $\lambda_0$  of these photons is scattered (rather than absorbed) by the medium, and after this scattering  $G_1$  of them escape from the system; one then gets for the fraction of photons that escape the medium after one scattering,  $P_1 = (1 - P_0)\lambda_0 G_1$ . Among the remaining part,  $\lambda_1$  of them experience a second scattering and  $G_2$  of them escape the medium after this scattering, so  $P_2 = [(1 - P_0)\lambda_0(1 - G_1)]\lambda_1 G_2$  of the photons escape the medium after two scatterings, and so on. We finally get the complete expression for the series of  $P_n$  (Eq. (6) of Y97)

$$P_n = \left( \prod_{i=0}^{n-1} \lambda_i - \sum_{j=0}^{n-1} P_j \prod_{i=j}^{n-1} \lambda_i \right) G_n. \quad (\text{B3})$$

For photons with initial energy  $E_0$ , define a dimensionless wavelength  $y_0 = m_e c^2 / E_0$ , where  $m_e$  is the mass of the electron and  $c$  is the speed of light. After  $n$  scatterings, if the fraction of the scattered photons have wavelength between  $y$  and  $y + dy$  is  $F_n(y, y_0)dy$ , then the energy distribution of photons that escape the medium after  $n$  scatterings is

$$N_n(E) = \int_E^{E_{\max}} dE_0 N_i(E_0) P_n F_n(y, y_0) \frac{dy}{dE}. \quad (\text{B4})$$

$E_{\max}$  is an upper limit set by the fact that photons with energy above this limit cannot reach energy  $E$  after  $n$  scatterings. It is convenient to change the integration variable  $E_0$  into  $y_0$ ; in this case we get (Eq. (7) in Y97),

$$N_n(E) = \frac{m_e^2 c^4}{E^2} \int_{y-2n}^y P_n F_n(y, y_0) N_i \left( \frac{m_e c^2}{y_0} \right) y_0^{-2} dy_0, \quad (\text{B5})$$

where  $y - 2n$  corresponds to the maximum energy that the initial photons contribute to photons with energy  $E$ , and it is determined by the fact that the maximum wavelength change per scattering is 2 (Y97).

The remaining task is then to determine the expressions of  $F_n$  and  $P_n$  (or  $\lambda_n$  and  $G_n$ ) in Eq. (B5). The non-relativistic approximation of  $F_n$  could be found in Sec. A.1 of Burigana (1995):

$$F_1 = \frac{3}{8}[1 + (\Delta y - 1)^2], \quad (\text{B6})$$

where  $\Delta y = y - y_0$ ;

$$F_2 = \begin{cases} f(\Delta y) & 0 \leq \Delta y < 2, \\ f(4 - \Delta y) & 2 \leq \Delta y < 4, \\ 0 & \text{otherwise,} \end{cases} \quad (\text{B7})$$

where  $f(\Delta y)$  is expressed as

$$f(\Delta y) = \left(\frac{3}{8}\right)^2 [4\Delta y - 4(\Delta y)^2 + 2(\Delta y)^3 - (\Delta y)^4/3 + (\Delta y)^5/30]; \quad (\text{B8})$$

and

$$F_n = \left(\frac{4\pi n}{5}\right)^{-1/2} \exp\left[\frac{-5(\Delta y - n)^2}{4n}\right] \quad n \geq 3. \quad (\text{B9})$$

The single-scattering albedo of photons with energy  $E$  is  $\lambda_0(E) = \tau_s/\tau_0$ . For photons with initial energy  $E_0$ , their wavelength distribution is  $F_n(y, y_0)$  after they are scattered  $n$  times by the medium. The albedo  $\lambda_n$  could then be represented by the mean of  $\lambda_0$  weighted by this wavelength distribution (Eq. (5) of Y97)

$$\lambda_n(E_0) = \int_{y_0}^{y_0+2n} \lambda_0(m_e c^2/y) F_n(y, y_0) dy. \quad (\text{B10})$$

The series of  $P_n$  in Eq. (B5) are obtained by recursion. First, the approximated expression of  $P_1$  that fits the Monte Carlo results is (Eq. (10) of Y97)

$$P_1 = \frac{A}{16J_1(\lambda_1, E_0)B}, \quad (\text{B11})$$

where  $A = \tau_s[4e^{-\tau_1} + 3e^{-\tau_0} + 2e^{-1/2(\tau_0+3\tau_1)} + 2e^{-1/2(\tau_0+\tau_1)} + 4e^{-1/2(\tau_0+\sqrt{3}\tau_1)} + e^{-(\tau_0+2\tau_1)}]$ ,  $B = 1 + 9.8600 \times 10^{-2}\tau_0 - 2.8717 \times 10^{-4}\tau_0^2 + 7.0954 \times 10^{-7}\tau_0^3$ , and  $\tau_1 = \tau_s/\lambda_1$ .  $J_1$  is the  $n = 1$  case of the series of (Eq. (11) of Y97)

$$J_n(\lambda_n, E_0) = e^{-\tau_s} + (1 - e^{-\tau_s})\lambda_n^{1/2(n-n_0+1)} \quad (\text{B12})$$

when  $n \geq n_0$  &  $E_0 > E_K$ , where  $n_0 = \max\{\text{int}[(E_K^{-1} - E_0^{-1})m_e c^2], 0\}$ , and  $E_K$  is the Fe K edge energies;  $J_n = 1$  otherwise.  $G_1$  is therefore determined according to Eq. (B3),

$$G_1 = \frac{P_1}{\lambda_0(1 - e^{-\tau_0})}, \quad (\text{B13})$$

and the expressions of the series of  $G_n$  are (Eq. (12) of Y97)

$$G_n = \frac{G_1[1 + e^{f(\tau'_n)}]}{J_n(\lambda_n, E_0)}, \quad (\text{B14})$$

where  $\tau'_n = \tau_s \lambda_{n-1} / (\lambda_0 \lambda_{n-2})$ ,  $f(\tau'_n) = \alpha_n + \beta_n e^{-\tau'_n / \gamma_n} + (0.25 + 0.75 e^{-\tau'_n / \gamma_n}) \ln \tau'_n$  is fitted to the Monte Carlo results. For  $n = 2$  to 9, parameters  $\alpha_n$ ,  $\beta_n$  and  $\gamma_n$  are listed in Table 1 of Y97, and  $G_{>9} = G_9$ .